Journal Pre-proof

Mechanical and morphological properties of parietal bone in patients with sagittal craniosynostosis

Sara Ajami, Naiara Rodriguez-Florez, Juling Ong, Noor ul Owase Jeelani, David Dunaway, Greg James, Freida Angullia, Curtis Budden, Selim Bozkurt, Amel Ibrahim, Patrizia Ferretti, Silvia Schievano, Alessandro Borghi

PII: S1751-6161(21)00560-9

DOI: https://doi.org/10.1016/j.jmbbm.2021.104929

Reference: JMBBM 104929

To appear in: *Journal of the Mechanical Behavior of Biomedical Materials*

Received Date: 21 November 2020

Revised Date: 15 October 2021

Accepted Date: 23 October 2021

Please cite this article as: Ajami, S., Rodriguez-Florez, N., Ong, J., Jeelani, N.u.O., Dunaway, D., James, G., Angullia, F., Budden, C., Bozkurt, S., Ibrahim, A., Ferretti, P., Schievano, S., Borghi, A., Mechanical and morphological properties of parietal bone in patients with sagittal craniosynostosis, *Journal of the Mechanical Behavior of Biomedical Materials* (2021), doi: https://doi.org/10.1016/j.jmbbm.2021.104929.

Mechanical and Morphological Properties of Parietal Bone in Patients with Sagittal Craniosynostosis

Sara Ajami [(1)], Naiara Rodriguez-Florez [(2,3)], Juling Ong [(4)], Noor ul Owase Jeelani [(4)], David Dunaway [(4)], Greg James [(4)], Freida Angullia [(4)], Curtis Budden [(4)] , Selim Bozkurt [(1,5)], Amel Ibrahim [(6)], Patrizia Ferretti [(1)], Silvia Schievano [(1)], Alessandro Borghi [(1)]

1. **UCL Great Ormond Street Institute of Child Health, London WC1N 1EH, UK**
2. **Universidad de Navarra, TECNUN Escuela de Ingenieros, Spain**
3. **Ikerbasque, Basque Foundation of Science, Spain**
4. **Craniofacial Unit, Great Ormond Street Hospital, London WC1N 3JH, United Kingdom**
5. **UCL Institute of Cardiovascular Science, London WC1E 6BT, UK**
6. **Biomaterials and Biomimetics, NYU College of Dentistry**

Abstract

Limited information is available on the effect of sagittal craniosynostosis (CS) on morphological and material properties of the parietal bone. Understanding these properties would not only provide an insight into bone response to surgical procedures but also improve the accuracy of computational models simulating these surgeries. The aim of the present study was to characterise the mechanical and microstructural properties of the cortical table and diploe in parietal bone of patients affected by sagittal CS. Twelve samples were collected from pediatric patients (11 males, and 1 female; age 5.2 ± 1.3 months) surgically treated for sagittal CS. Samples were imaged using micro-computed tomography (micro-CT); mechanical properties were extracted by means of micro-CT based finite element modelling (micro-FE) of three-point bending test, calibrated using sample-specific experimental data. Reference point indentation (RPI) was used to validate the micro-FE output. Bone samples were classified based on their macrostructure as unilaminar or trilaminar (sandwich) structure. The elastic moduli obtained using RPI and micro-FE approaches for cortical tables (E_{RPI} 3973.33 ± 268.45 MPa and $E_{micro\text{-}FE}$ 3438.11 ± 387.38 MPa) in the sandwich structure and diploe (E_{RPI}1958.17± 563.79 MPa and $E_{micro\text{-}FE}$ 1960.66± 492.44 MPa) in unilaminar samples were in strong agreement ($r=.86$, $p<0.01$). We found that the elastic modulus of cortical tables and diploe were correlated with bone mineral density. Changes in the microstructure and mechanical properties of bone specimens were found to be irrespective of patients' age. Although younger patients are reported to benefit more from surgical intervention as skull is more malleable, understanding the material properties is critical to better predict the surgical outcome in patients <1 year old since age-related changes were minimal.

Keywords: Craniosynostosis, Cranial bone microstructure, Biomechanics of cranial bone, Pediatric

1 Introduction

Craniosynostosis (CS) is a congenital malformation defined by premature fusion of one or more skull sutures – specialised fibrous joints which connect the bones of the cranial vault [1]. CS results in abnormalities of normal skull growth, causing aesthetic deformity and, in some cases, functional problems affecting relevant organs such as the brain and eyes. It can present as part of a genetically or clinically defined syndrome [2], but in the majority of CS patients no genetic cause is identified and only a single cranial suture is affected – so called 'non-syndromic CS [3, 4]. Sagittal CS is the most common type of CS accounting for between 40% and 55% of non-syndromic cases [3]. If untreated, skull malformations may result in functional problems such as intracranial hypertension, which may result in visual and neurological harm [5].

Currently, the only interventions for CS are surgical. Surgical techniques can broadly be divided into minimally invasive techniques, where the fused suture is released and distraction (internal or external) is applied; or calvarial vault remodelling procedures, more extensive operations where osteoplastic flaps are cut from the skull, reshaped and repositioned to correct head shape. Minimally invasive techniques such as spring-assisted cranioplasty (SAC) have become increasingly popular over the last 20 years, particularly in young infants, as they involve smaller skin incisions and less extensive soft dissection and osteotomies, with concurrent reductions in transfusion rates, length of hospital stay and post-operative recovery [6, 7]. However, the optimal timing of surgery for CS remains unclear and a subject of ongoing debate.

Previous studies have used FE and statistical shape modelling to predict final head changes and unveil surgical factors affecting the outcome [8-10]. While promising results have been reported, one of the difficulties in such models is the lack of information on the mechanical properties of the paediatric skull affected by CS [9]. Moreover, a recent study by Rodriguez-Florez et al. has suggested that when predicting surgical outcomes, preoperative examination of cranial bone structure should be considered for patients with an age range of 3-8 months, as the bone structure strongly affects head shape changes in patients [11]. The structure of the cranial bone evolves from unilaminar structure in childhood to trilaminar (sandwich) structure in adults: during growth, the cranial bone differentiates structurally into a three-layer composite consisting of two external cortical tables and a central trabecular layer, the diploe [12-14]. Florez et al. reported parietal bone samples with unilaminar structure were associated with an increased improvement in head shape changes than trilaminar [11].

The parameters indicative of bone quality are not accurately interpretable from clinical examination and traditional radiographic imaging approaches, and often rely on ex-vivo

techniques to quantify the changes. The ability to non-invasively measure the material level changes in vivo that relates to bone pathophysiology represents a powerful tool for disease diagnosis and management [15-20]. Therefore, there is an immense desire for non-destructive biomarkers to characterise bone properties. The aim of this study was to characterise the microstructural and mechanical properties of parietal bone in paediatric patients with sagittal CS and to identify a translatable biomarker representative of bone properties in order to better predict surgical outcomes. Bone samples were classified as unilaminar or trilaminar. Since the cortical and diploe feature independent mechanical properties and architecture, an enhanced characterisation of each layer was carried out to improve our understanding of changes in the diseased cranial bone. Micro-computed tomography (micro-CT) based finite element (micro-FE) modelling has been widely used to indirectly assess the biomechanical properties of bone and is particularly attractive as a tool to evaluate bones when physical testing of samples is not possible [21-25]. On the other hand, a common method for direct bone testing is reference point indentation (RPI), which is a non-destructive approach to test bone material properties using cyclic micro-indentation [26]. Microstructural properties of the cranial bone were examined using high-resolution micro-CT; three-point bending tests were carried out on each sample and the output was used to calibrate micro-FE model which allowed reverse estimation of each layer's mechanical properties; finally, validation of the results was carried out against RPI.

2 Materials and Methods

2.1 Sample collection and preparation

In this study 12 patients (1 female and 11 males, age = 5.2 ± 1.3 months, ranging between 3 and 8 months) affected by non-syndromic, sagittal CS who underwent SAC at Great Ormond Street Hospital for Children (GOSH, London, UK) between November 2018 and June 2019 were prospectively recruited. SAC is the standard of care in GOSH for the correction of scaphocephaly in young children affected by single-suture sagittal CS. Detailed information on the surgical procedure can be found at Rodgers et al.[6]. As a part of the procedure, a square craniectomy is performed straddling the sagittal sinus approximately halfway along the fused sagittal suture, with the cranial bone fragment being usually discarded. Following ethical approval and parental consent (UK Health Research Authority REC reference: 09/H0722/28) the excised bone specimens, namely parietal bones, were collected from the operation. Retrieved bone samples were cleaned of soft tissue, fixed in 4% paraformaldehyde (PFA) for 24 hours, and stored in -20°C freezer until preparation for testing.

2.2 Micro-computed tomography (micro-CT)

Parietal bone samples were thawed in phosphate buffered saline (PBS) at room temperature for less than 3 hours prior to micro-CT scanning. Each sample was scanned using a Skyscan 1172 (Skyscan, Kontich, Belgium) at a voxel size of 8.9 µm, with an X-ray tube operated at 49 kV, 200 µA, 885 ms exposure time, a rotational step of 0.4°over 180° total rotation, and a 0.5 mm aluminum filter. The slices were reconstructed using NRecon 1.7.1.0 (Skyscan, Kontich, Belgium). 2D/3D analyses were performed using CTAn software (Skyscan, Kontich, Belgium). Finally, CTvox (Skyscan, Kontich, Belgium) was used for 3D visualisation and production of colour-coded images of trabecular thickness and separation.

A visual inspection of the micro-CT images demonstrated that the structure of parietal bone samples was either unilaminar (n=6) composed of diploe or trilaminar (n=6) with an outer and inner cortical table and a diploe core. Calibrated micro-CT was used to assess trabecular bone mineral density (BMD) and cortical tissue mineral density (TMD) using two SkyScan-supplied bone phantoms with known mineral density values of 0.25 and 0.75 g/cm^3 calcium hydroxyapatite. The phantoms were scanned and reconstructed using the same scan settings.

2.3 Sample beam mechanical testing

Beam-shaped specimens were cut from the parietal bone, parallel to the sagittal suture and under constant irrigation at room temperature using a diamond saw (Isomet™, Buehler,

Coventry, UK), with a target width of 2 mm. The beams were placed on a custom-made fixture with adjustable span in a manner consistent with simply supported boundary condition and loaded midspan. A span length of 10.40 or 5.40 mm was used. Different lengths were chosen due to the restrictions in the size of the sample available.

The samples were subjected to a three-point bending test using a Zwick Roell material testing machine (Z0.5, Zwick Roell Group, Ulm, Germany) at 0.005 mm/s for 4 cycles up to a maximum deflection of 0.5 mm. During the test, the force-displacement curves were recorded and used later for calibration of the micro-FE model and indirect estimation of the calvarial bone material properties.,.

2.4 Micro-Finite Element Modelling (Micro-FE)

3D CAD models of bone samples were generated from the reconstructed micro-CT images (Figure 1). Each image-set was imported into ScanIP software (version N-2018.03, Simpleware Ltd., Exeter, UK). The image datasets were subsampled to a pixel size of 20 µm to remove un-necessary detail and help with mesh creation. In each dataset, the regions representing the parietal bone were segmented using a combination of threshold and flood fill operations to remove any floating or disconnected structures. Three different volumes of interest (VOI) in the shape of rectangular beams matching the dimensions of the beam used for the mechanical test were extracted from each dataset to examine intrasample variability (Figure 1B). The selected beams were in the same or close to the location of the beam prepared for experimental three-point bending. Therefore, it can be assumed that the FE model would well represent the beam tested experimentally. In each beam, cortical compartment and diploe were manually segmented according to macro-porosity (Figure 1C): cortical bone shows a compact structure with low porosity; trabecular bone shows a lattice-type and highly porous structure. We inversely characterised the Young's modulus of the diploe in unilaminar, cortical and diploe in trilaminar structures, using micro-FE model of three-point bending - calibrated with three-point bending experimental output. A design of Experiment stage followed by model optimization (using Latin hypercube sampling design algorithm implemented in ANSYS - Release 19.0, ANSYS, Inc. and ANSYS Europe, Ltd.) allowed the estimation of the different layer mechanical properties by matching the mechanical response of the micro-FE model (displacement vs reaction force) with the relative curve retrieved during the three-point bending test. The outer layer properties (diploe in the unilaminar samples, cortical layer in trilaminar samples) was compared with RPI measurements for validation.

Symmetry within the beam was assumed, to simplify the use of boundary conditions and to decrease the computational time. A comparison with the numerical results between the full beam and quadrant beam models was carried out in 4 samples and a deviation of less than 10% was found. Then a quadrant from each beam was used to build tetrahedral meshes (SimplewareFE, version N-2018.03, Simpleware Ltd., Exeter, UK) with a coarseness value of -25, which corresponded to an average of 98,182 nodes (17,927 nodes/mm^3) and 381,530 elements (69,191 elements/mm^3) for all patients and imported to ANSYS to simulate bending using the same conditions as the mechanical testing (supplementary materials). A mesh sensitivity analysis on element size was performed on 4 samples to achieve optimal balance between accuracy (with a deviation threshold of 5%) and CPU time. For all micro-FE models, the bone material properties were considered to be isotropic, linear elastic, and uniform with a Poisson's ratio of 0.3. The loading point and support were simulated using displacement conditions on specific node subsets (linearly increasing displacement from 0 to 0.5mm for the loading point, while imposing zero displacements for the support). The diploe and cortical moduli were determined using a response surface optimisation method targeting the peak force obtained in experimental testing with an error percentage of less than 0.5.

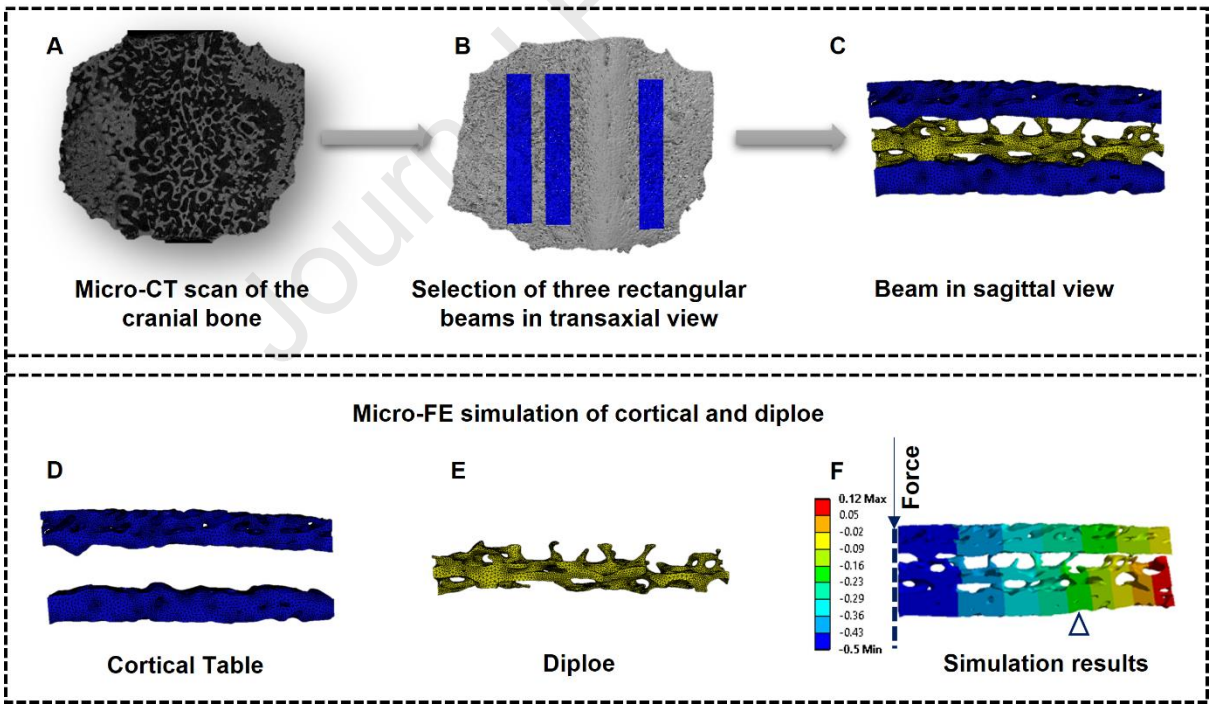

Figure 1. An Overview of operational steps performed for micro-FE modelling of three-point bending in parietal bone samples. The sample presented in this figure is representative of a parietal bone with trilaminar structure. A) Parietal bone samples were collected from craniosynostosis patients and scanned with micro-CT; (B) Reconstructed micro-CT images were imported into ScanIP software and three rectangular beams were excised; (C) Rectangular beams with trilaminar (sandwich) structure were segmented into (D) cortical tables and (E) diploe compartments and meshed for subsequent (F) micro-finite element analysis.

2.5 Morphometric Analysis

Each resized dataset was imported into CTAn for morphological analysis [27]. The measured structural parameters for all samples (unsegmented) were bone volume fraction (BV/TV; %), specific bone surface (BS/BV; mm^{-1}), Cs.Th (cross-sectional thickness; mm) and bone mineral density (BMD, g/cm^3). For the diploe analysis BV/TV, BS/BV, Cs.Th, BMD, trabecular thickness (Tb.Th; mm), trabecular number (Tb.N; mm^{-1}), trabecular spacing (Tb.Sp; mm), bone pattern factor- index of trabecular bone connectivity (Tb.Pf; mm^{-1}), and porosity (Po ;%) were determined. For cortical bone, BV/T, BS/BV, Po, and tissue mineral density (TMD, g/cm^3) were analysed.

2.6 Reference Point Indentation (RPI)

Microindentation was performed using an RPI system (BioDent; Active Life Scientific, Santa Barbara, CA, USA). Briefly, RPI measures the displacement (relative to the bone surface) of a stainless steel test probe that indents the bone at a given load, dwells for a short period (typically <200 ms), and unloads to ~0 N [26]. The probe assembly consists of a cannula-like reference probe and a test probe that slides inside the reference probe. This allows the reference probe to establish and maintain a reference point on the material enabling the test probe to precisely indent the material relative to that established reference point. Each indentation was performed using the BP2 probe (375 µm diameter, 90° cono-spherical, 5 µm radius tip) and consisted of 10 cycles at 2 Hz with a maximum force of 2 N per cycle. Measurements were repeated at 5 regions per sample and each indentation site was approximately 5 mm apart (spacing between the indentation was >3 times the indent diameter [28]). Throughout the testing, specimens were kept moist with PBS at room temperature. Prior to testing, probes were calibrated using polymethylmethacrylate (PMMA) according to the manufacturer's instruction [29, 30].

RPI output was used to calculate the elastic modulus of diploe ($E_{\text{Diploe unilaminar}}$) in unilaminar samples and cortical bone ($E_{\text{Cortical trilaminar}}$) in trilaminar structures. The elastic modulus was calculated using the Oliver–Pharr technique [31]: initially, the reduced elastic modulus (E_r) was calculated using the equation shown below:

$$E_r = \frac{\sqrt{\pi}S}{2\sqrt{A}}$$

where S is the unloading slope when maximum indentation force is reached and A is the contact area, which is the projected area geometry of the cono-spherical tip calculated from radius and the contact depth of the indenter.

$$Area = \pi\left((r \times 0.414) + Indentation\ Depth\right)^2$$

From the reduced elastic modulus, the bone elastic modulus was computed:

$$\frac{1}{E_r} = \frac{1 - \upsilon^2}{E} + \frac{1 - \upsilon_i^2}{E_i}$$

where E and ν (0.3) are the elastic modulus and Poisson's ratio for the bone and E_i (200GPa) and ν_i (0.3) are the same parameters for the indenter.

2.7 Statistical analysis

All Statistical analyses were performed using SPSS 25.0 (SPSS, Inc., Chicago, IL, USA). Results are presented as mean ± standard deviation. Mann Whitney U test was used to assess the statistical significance of the differences between cortical tables and diploe. The correlation between the mechanical properties and microstructural parameters of the bone samples, and the agreement between RPI and micro-FE approaches were evaluated using Spearman's rank correlation. Results were considered significant when $P<0.05$.

3 Results

3.1 Biomechanics of Parietal Bone in Patients with sagittal CS

A total of 12 samples were collected from pediatric patients representing unilaminar (n=6) and trilaminar (n=6) structure. The elastic modulus obtained for parietal bone was determined using RPI and micro-FE model of three-point bending.

RPI allowed calculation of superficial layer Young's modulus, hence cortical Young's modulus for the trilaminar structure ($E_{Cortical\ trilaminar}$) and diploe for the unilaminar structures ($E_{Diploe\ unilaminar}$). The average total indentation distance (TID) in the cortical layer of trilaminar samples (36.25 ± 3.56 µm) was much lower than the average thickness of the cortical layer (269.47±75 µm) in all samples. A significantly higher elastic modulus for the cortical bone in trilaminar structures was found in comparison to diploe ($E_{Cortical\ trilaminar}$ 3973.33 ± 268.45 MPa vs $E_{Diploe\ unilaminar}$ 1958.17± 563.79 MPa, $p<0.01$) in unilaminar structure (supplementary materials). The average TID and unloading slope were: 53.33 ± 8 µm and 0.24 ± 0.06 N/µm for unilaminar samples and 36.25 ± 3.56 µm and 0.31 ± 0.03 N/µm for trilaminar samples ($p<0.05$).

Micro-FE allowed indirect evaluation of bone Young's modulus by means of model optimization; when all bone samples were initially treated as a homogeneous material (cortical layer and diploe treated as same), an average value of 1412.16 ± 539.11 MPa (range; 729.69 – 2416.98) was derived. When the cortical layer was separated from diploe in the subset of patients who had a trilaminar structure, the values indicated that Young's modulus of the diploe layer in unilaminar structures was lower than the cortical ($E_{Cortical\ trilaminar}$ 3438.11 ± 387.38 MPa vs $E_{Diploe\ unilaminar}$ 1960.66± 492.44 MPa, $p<0.01$) but higher than the diploe ($E_{Diploe\ unilaminar}$: 1960.66± 492.44 vs $E_{Diploe\ trilaminar}$ 651.13 ± 331.35 MPa, $P<0.01$) in trilaminar structures.

The level of agreement between the micro-FE and RPI data for cortical and diploe is illustrated in Figure 2. Spearman's correlation, used to assess the relationship between $E_{Micro\text{-}FE}$ and E_{RPI}, confirmed a strong correlation ($r=.86$, $p<0.01$). There were no significant correlations between age and the elastic modulus of samples (Figure 3).

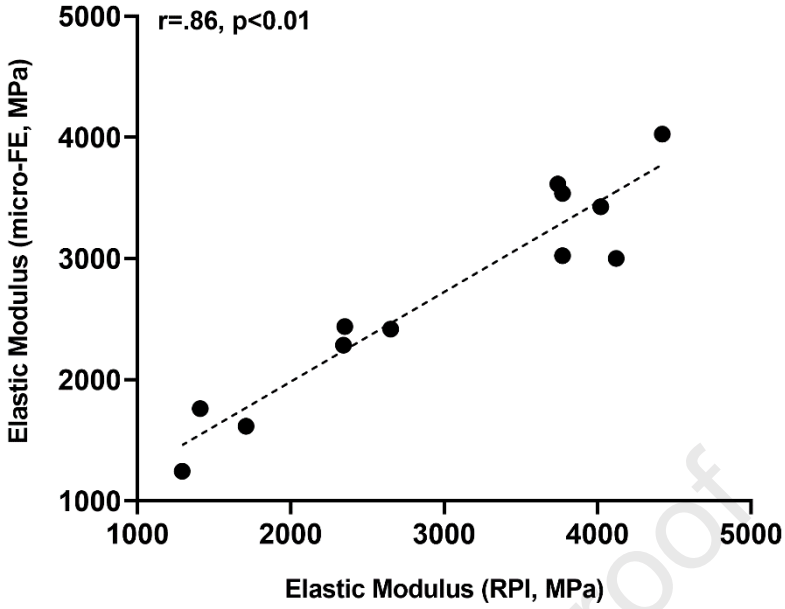

Figure 2. Correlation between elastic modulus derived from reference point indentation (RPI) and micro-FE models. The cortical modulus from trilaminar samples and diploe modulus from unilaminar samples were considered. Strong, positive correlation was found between $E_{micro-FE}$ and E_{RPI}.

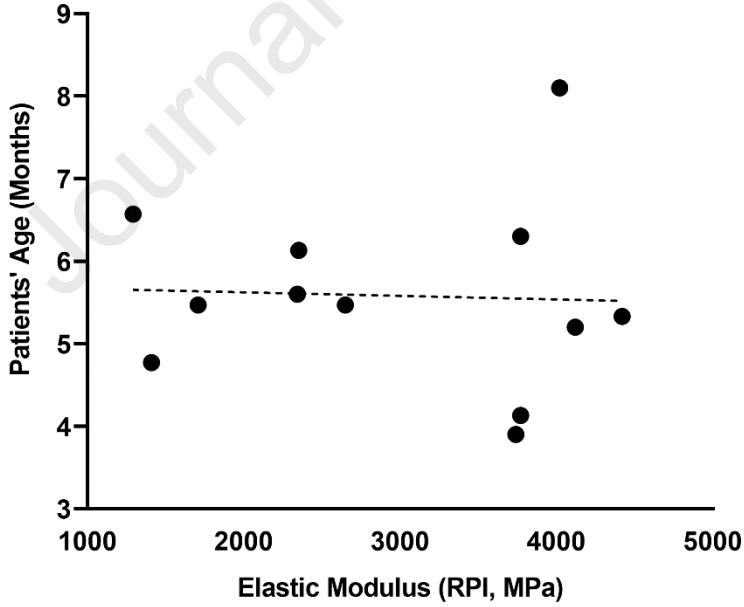

Figure 3. Relationship between patients' age and elastic modulus obtained from reference point indentation. For trilaminar samples the modulus for cortical tables and, for unilaminar the modulus for diploe were considered. No significant correlations were found.

3.2 Sagittal CS and Microstructure of Parietal Bone

Figure 4 represents differences in the macrostructure of micro-CT scanned parietal bones between patients. A sandwich structure was observed in six patients with a mean age of 5.5 ± 1.5 months (range; 3-8), whereas the other six with a mean age of 5.7 ± 0.6 months (range; 4-6) represented a unilaminar diploe structure. No statistical differences were found when the age of patients in the two subgroups was compared.

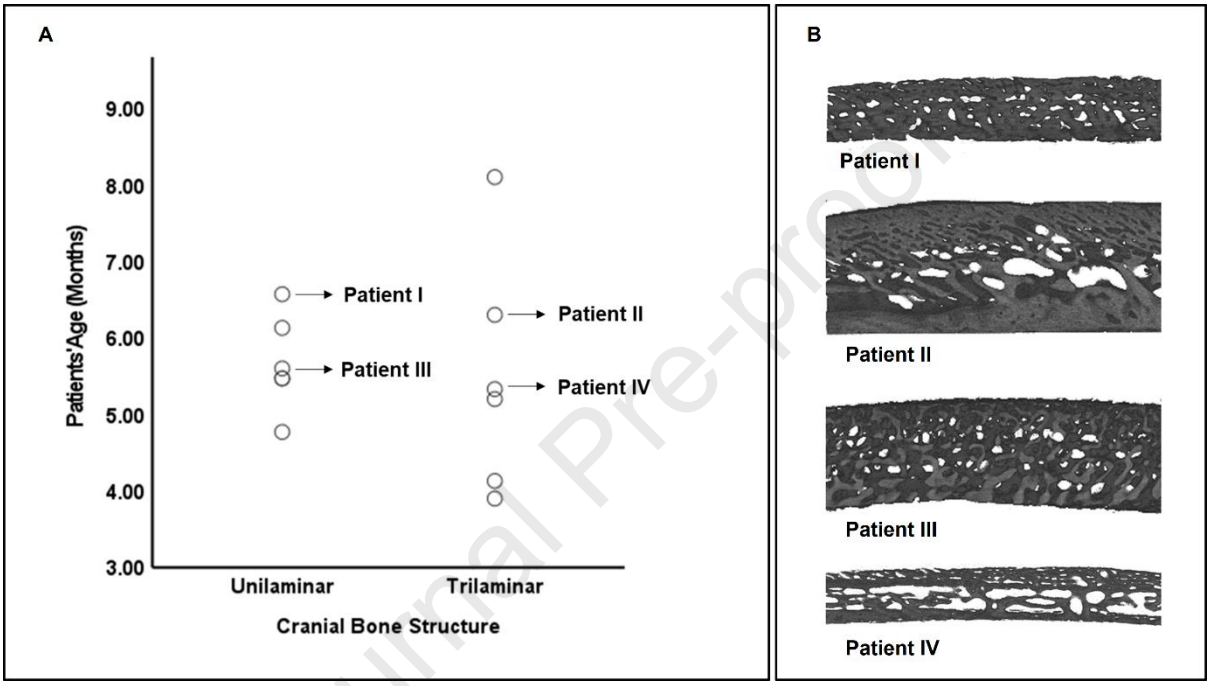

Figure 4. Age is not the sole representative of cranial bone macrostructure in patients with sagittal craniosynostosis. (A) Variation in macrostructure of cranial bone in 3-8 months old patients. (B) Representative micro-CT images of retrieved parietal bone samples. 3D visualization of unilaminar structure in (I) 6.5 month old and (III) 5.6 month old patients; and trilaminar structure in (II) 6.3 month old and (IV) 5.3 month old patients.

The 3D microstructure of all samples was examined regardless of their structure. The mean cross-sectional thickness for all samples was 1.32 ± 0.29 mm. The average BV/TV, BS/BV, porosity and BMD were respectively 59.63 ± 11.23 %, 16.50 ± 4.90 mm^{-1}, 40.37 ± 11.23 % and 1.34 ± 0.29 $g.cm^{-3}$. When the microstructure of the parietal bones with sandwich structure was compared with the unilaminar samples, a significantly higher BS/BV was found in unilaminar samples (20.14 ± 3.40 vs 12.87 ± 3.08 mm^{-1}, p=.01). Porosity was also higher in unilaminar parietal bone specimens in comparison to sandwich structure, although it was not statistically significant (43.24 ± 13.43 vs 37.49 ± 8.79 %). A trend towards increasing in BMD from unilaminar to trilaminar bone structure (1.19 ± 0.21 $g.cm^{-3}$ vs 1.49 ± 0.29 $g.cm^{-3}$, p=.09) was observed. A similar trend was observed when cross-sectional thickness (unilaminar 1.22

± 0.29 mm vs trilaminar 1.43 ± 0.27 mm) and BV/TV (unilaminar 56.76 ± 13.43 % vs trilaminar 62.51 ± 8.79 %) in unilaminar and trilaminar samples were compared.

The 3D analysis of diploe segmented from the trilaminar structure (diploe $_{trilaminar)}$ and unilaminar (diploe $_{unilaminar}$) samples showed no significant differences when BV/TV (unilaminar 56.76 ± 13.43 % vs trilaminar 50.49 ± 8.11 %) and BS/BV (unilaminar 20.14 ± 3.40 mm^{-1} vs trilaminar 18.66 ± 2.28 mm^{-1}) were compared. The diploe in the unilaminar structure was significantly thicker in cross section when compared to diploe from trilaminar structure (unilaminar 1.22 ± 0.28 mm vs trilaminar 0.77 ± 0.24 mm, p=.01). A significantly thicker (unilaminar 0.18 ± 0.02 mm vs trilaminar 0.21 ± 0.02 mm, p=.04) and more separated (unilaminar 0.22 ± 0.09 mm vs trilaminar 0.34 ± 0.05 mm, p=.04) trabeculae was found in the trilaminar structure when compared to the unilaminar structure (Figure 5). No significant differences were found when the trabecular number (unilaminar 3.26 ± 0.66 mm^{-1} vs trilaminar 2.48 ± 0.30 mm^{-1}) and porosity (unilaminar 43.24 ± 13.43 mm^{-1} vs trilaminar 49.51 ± 8.11 mm^{-1}) was considered. Analysis of Tb.Pf revealed a concave and convex structure respectively in unilaminar and trilaminar structure (unilaminar -0.12 ± 3.33 mm^{-1} vs trilaminar 4.27± 1.99 mm^{-1}, p=.03). When comparing the BMD no significant differences were found (unilaminar 1.19 ± 0.21 vs trilaminar 1.13 ± 0.32 $g.cm^{-3}$). Overall, an increase in BV/TV was associated with dense (r=.71, p=.01) and a high number of trabeculae (r=.81, p<0.01) with a significant reduction in BS/BV (r =-.59, p=.04), Po (r=-1, p<0.01), Tb.Sp (r=-.74, p=.01), and Tb.Pf (r=-.73, p=.01). Parietal bone samples with larger cross sections had a thinner trabeculae (r=-.59, p=.04). BS/BV had a significant positive correlation with Po (r=0.6, p=0.04), and negative correlation with Tb.Th (r=-.78, p<0.01) and BMD (r=-.64, p=.03). Moreover, the higher the trabecular number the more separated they were (r=-.85, p<0.01). Tb.Pf was significantly negatively correlated with BV/TV (r=-.73, p=.01) and Tb.N (r= -.69, p=.01).

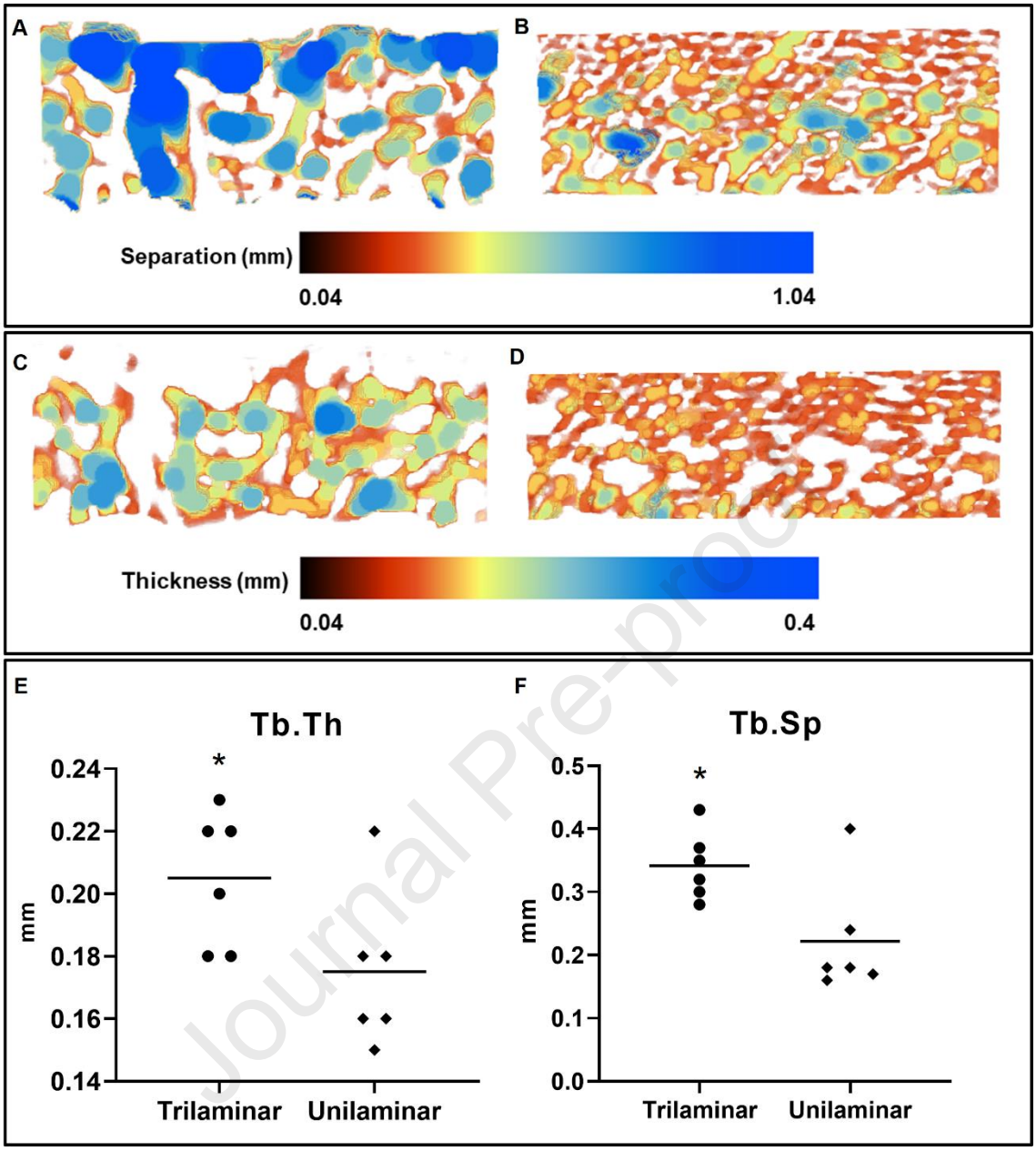

Figure 5. Diploe structure in paediatric patients with craniosynostosis. Representative colour-coded images of trabecular separation in (A) trilaminar and (B) unilaminar structures. Representative colour-coded images of trabecular thickness in (C) trilaminar and (D) unilaminar structures. Trabecular thickness (E) and trabecular separation (F) were significantly higher in trilaminar samples compared to unilaminar. Statistical comparisons: * denotes $p \leq 0.05$.

Assessment of the cortical morphology showed a BV/TV of 71.09 ± 8.61% (range; 59.91-81.77) which was statistically negatively correlated with BS/BV 12.88 ± 3.17 mm^{-1} (range; 9.36-16.46; r= -.88, p=.02) and total porosity 28.91 ± 8.61% (range; 18.23-40.09; r= -1.00, p<0.01). An increase in TMD 2.30 ± 0.19 $g.cm^{-3}$ (range; 1.94 - 2.46) was positively correlated with BV/TV and had a significant negative correlation with BS/BV (r= -.83, p=0.04). No correlations were found between the microstructural properties and age.

3.3 Elastic modulus of the parietal bone is related to specific architectural parameters

The elastic modulus of the cortical bone segmented from trilaminar structure and diploe from unilaminar structure measured by RPI and FEA was positively correlated with bone mineral density (E_{RPI}; r=.57, p= .05 and $E_{micro\text{-}FE}$; r=.64, p=.03). $E^{diploe}_{micro\text{-}FE}$ for all 12 samples increased significantly with a decrease in trabecular thickness (r=-.61, p=.03), and Tb.Pf (r=-.73, p=.01).

4 Discussion

Surgical procedures performed for the management of sagittal CS are highly variable between centres and there is no consensus in the literature regarding optimal surgical treatment. Regardless of the surgical approach employed, most clinicians advocate for surgical intervention within the first year of patients' life to take advantage of skull malleability and rapidly expanding brain to drive optimal remodelling of the skull [32, 33]. At Great Ormond Street Hospital, we favour minimally invasive SAC [6, 8], safe and successful in expanding the skull, but sometimes with suboptimal shape results. Age alone cannot explain the changes in the final morphological SAC outcome [11]. Previous studies have focused on understanding the pathogenesis of the disease, whilst material and morphological properties of cranial bone in patients affected by CS remain unknown. In this study, we characterised the microstructure and mechanical properties of parietal bone retrieved from sagittal CS patients. Initially bone samples were scanned with micro-CT. A rectangular beam was then prepared from each specimen for experimental three-point bending and RPI. Following that, micro-CT datasets were used to generate micro-FE models of three-point bending. For each sample three beams matching the dimensions of the beam used for the experimental three-point bending test were extracted (from the micro-CT datasets) to examine intrasample variability. Using micro-FE model of three-point bending, calibrated using three-point bending experimental data- we inversely characterised the young's modulus of the diploe in unilaminar, cortical and diploe in trilaminar structures. To validate such inverse characterisation step, we compared the superficial Young's modulus retrieved using RPI and we found very good matching in both unilaminar (micro-FE vs diploe RPI) and trilaminar (micro-FE vs cortical layer RPI).

Three-point bending test is one of the most common approaches to examine biomechanical properties of whole bone [34-36]. Several assumptions underlie the use of beam theory to calculate the elastic modulus of bone including a beam with uniform cross-section, homogenous isotropic material, and a high length to depth ratio (a ratio of over twenty for bone samples) [37, 38]. These assumptions have been identified as a potential source of errors when testing short specimens as the bending test will generate a larger shear deformation in addition to bending deformation thus reducing the value of Young's modulus derived from the test [39-41]. In order to overcome these limitations, micro-FE models can be used to determine the mechanical properties of bone samples. In the present study, to take into account the complexity of parietal bone structure and provide an insight into non-invasive methods for determining the elastic modulus of the parietal bone, samples were micro-CT scanned and micro-FE models were generated. We showed that the elastic modulus of the entire beams calculated from micro-FE models were 1412.16 ± 539.11 MPa. In comparison to the literature,

this is the first study to investigate the mechanical properties of cranial bone in CS patients. Few studies have reported the mechanical properties of adult and infant cranial bone [42-47]. Coats and Margulies tested human infant (<1 year old) cranial bone in three-point bending at test rates of 1.58 and 2.81 m/sec and found an elastic modulus of 461 MPa for parietal bone [45]. Wang et al reported an elastic modulus of 1103.01 MPa for parietal bones in 1-2 year old infants [48]. Margulies et al. investigated the age-dependent changes in skull properties in a bending set up. The reported elastic modulus for parietal bone ranged from 71.6 MPa at 25 weeks gestation to 3582.2 MPa at 6 months term [49].

For micromechanical characterisation of cortical and diploe, micro-FE derived moduli were compared with RPI. Good correlation was found in the past between RPI / micro-indentation profiles and the respective finite element simulations [50, 51], hence in this work, the modelling was restricted to the simulation of the three-point bending to account for the differences in stiffness between the cortical and the diploe layers in the trilaminar samples. While RPI experimental values validated the micro-FE indirect estimation of surface stiffness for unilaminar and trilaminar samples, model optimization allowed robust estimation of the stiffness of the diploe layer, which well compared with literature values [48, 49, 52]. The three-layer moduli could be used in FE simulations which explicitly model the three layers of the sandwich structure of the skull [53]. Results from RPI and micro-FE approaches were in strong agreement with each other. Peterson and Dechow examined the cortical material properties of human parietal bone in an age range of 58-88 years [54]. A longitudinal modulus (E_1) with grand means of 10.6 GPa for the inner and 13 GPa for the outer table was found. Davis et al. loaded 47 samples from one six year-old human cranium to failure via four-point bending and reported an elastic modulus of 9.87±1.24 GPa for cranial cortical bone [55]. The moduli found for the cortical tables in our study using RPI and micro-FE were respectively 3973.33 ± 268.45 MPa and 3438.11 ± 387.38 MPa. The modulus of the diploe ($E_{\text{Diploe unilaminar}}$ 1958.17± 563.79 and $E_{\text{Diploe trilaminar}}$ 651.13 ± 331.35 MPa) in this study falls within the 0.4 to 2.8 GPa range reported by Melvin et al. [52] for bones tested in compression. To the author's knowledge, no information is available on the mechanical properties of the cortical tables and diploe in the fetal population.

The variability in the structure of the bone (unilaminar or trilaminar) is associated with the magnitude of final head shape changes after SAC [11]. Therefore, we have reviewed various morphological parameters to identify an imaging biomarker that would represent the bone structure. We found that bone macrostructure was not reflective in the sample cross-sectional thickness and BMD. Although parietal bone specimens with the sandwich structure were generally thicker with increased BMD when compared to unilaminar types, no significant

differences were found. This can be due to the limited number of samples examined here. Florez et al. [11] reported parietal bone samples with sandwich structure was significantly thicker than the samples with a unilaminar structure. When patients' age was considered, no correlations were found with thickness (range; 0.82 – 1.88 mm) and BMD (range; 0.92-1.84 $g.cm^{-3}$). The postnatal growth of the calvarium occurs rapidly during the first year followed by a reduced growth rate until the skull approaches adult size at approximately the age of 7 [56]. In non-CS infants, parietal bone thickness with a median of 1.45 mm in the age group of 3-6 months, 1.69 mm in the age group of 6-9 months, and a mean of 3.4 -4.1 mm in the age group of 0-12 months were reported using CT and histological analysis [12, 57]. Since the changes in cranial thickness correlate with occipitofrontal circumference and cephalic index [11, 12, 58], determining the thickness and in-depth understanding of factors affecting it such as gender [59], ethnic origin [60] and anatomical site [59, 61] would aid predicting the final head shape outcome. Our data showed that age is not a significant predictor of parietal thickness for the cohort examined. A minimum thickness of 0.82 mm and a maximum of 1.88 mm was found respectively for 4.7- and 4.1-month-old patients. This variation in the thickness might be due to the remodelling of the bone and changes in the microstructure as a result of the disease. Moreover, no age-related changes in the macrostructure of the samples were found (Figure 4) and patients of the same age were identified with different bone structures. A 6.5 month old patient was represented with unilaminar diploe, whilst a sandwich structure was found in a 6.3 month old patient. This is in line with previous findings from our group on the cranial bone structure of sagittal CS [11]. Further research is required to study the longitudinal structural changes of the non-diseased cranial bone to investigate how CS interferes with the developmental timeline. It must be noted that in this study all the parietal bone samples were harvested from the same anatomical site.

Gender is one of the important risk factors in sagittal CS, affecting 3.5 males for every 1 affected female [62-65]. In our study, the effect of gender was not considered as 11 male patients were compared to 1 female patient. The role that gender may play in predisposing an individual to certain forms of CS has been of interest. It has been suggested that the male predominance in certain forms of CS is attributable to a larger head circumference in male fetuses resulting in a higher degree of intrauterine constraint [66, 67], while in other studies higher levels of circulating serum androgens [68], dysregulation of osteoblast differentiation and genetic factors were demonstrated to contribute to development of sagittal CS and gender related differences [69]. There is limited research available on how the gender difference can affect the material and morphological properties of bone. Future research should address this further.

Previous studies have shown that micro-CT scanning voxel size affects the cortical and trabecular bone microstructure if the voxel size is not appropriately small compared to the dimensions of the structure being measured [27, 70, 71]. The microstructural properties of the bone samples in this study were determined at the same 20 µm resolution that the CAD models were generated in order to minimise the error when investigating the correlation between the microstructural and mechanical properties of the samples in the micro-FE model. In a previous publication by our group [11], when parietal bone samples were scanned at isotropic voxel sizes of 5–8 µm (equivalent to an approximate resolution of 6–9 µm) a BV/TV of 50 ± 10% was found compared to our current findings : 59.63 ± 11.23 %.

The mechanical response of the cranial bones may be highly sensitive to their corresponding microstructure [13]. Our findings indicated that the unilaminar samples represented a more separated and thicker diploe with a reduction in their corresponding micro-FE derived elastic modulus when compared to trilaminar specimens. The trilaminar parietal bone is analogous to an engineering sandwich structure, which is composed of stiff cortical tables (micro-FE 3438.11 ± 387.38 MPa) and energy absorbing porous lightweight diploe (micro-FE 651.13 ± 331.35 MPa). Zhai et al reported that the thickness ratio of the diploe to the entire sandwich structure plays an important role in determining the strength in a tangential direction [72]. For both RPI and micro-FE approaches, the elastic modulus of segmented cortical tables and diploe correlated well with tissue and bone mineral density measured by micro-CT. Cortical porosity is one of the most important predictors of bone strength and has been reported to be negatively correlated with elastic modulus [73-75], although we did not find any significant correlations. Previous studies have captured vascular porosity when voxel size of 41 and 82 µm were used to scan human tibiae [76] and radii [77]. Therefore, the cortical porosity determined in our study at 20 µm resolution may be representative of vascular porosity. Further research using histological and high-resolution micro-CT is needed to confirm that as limited information is available in the literature on the microstructure of parietal bone from paediatric patients,

The radiation dose used here for imaging and micro-FE modelling of the samples were too high for clinical applications. Hence, it highlights the need for translatable imaging biomarkers. Our results indicated that bone mineral density and cross-sectional thickness should be further investigated as a potential imaging biomarker in the clinical assessment of sagittal CS for identifying the macrostructure and evaluating the mechanical properties. Previous studies have indicated that Hounsfield unit (HU) values obtained from computed tomography (CT) scans can be used for determining regional BMD through calibration using a phantom with known bone mineral density [78-81]. In a recent study by Delye et al. BMD of the cranial bone

was determined in 187 patients (age range 0–20 years old) based on the average number of HUs of skull models processed from CT data [57].

This study has a few limitations that should be taken into consideration when interpreting the results. First, the parietal bone specimens were fixed in PFA. Long term embalming of bone samples has been shown to significantly affect their mechanical properties [82]. Although the parietal bones here were not stored in PFA for long period, further studies are required to address the effect of our preservation method on their material properties. Second, the influence of the cortical site (inner or outer table) was not taken into consideration when tested with RPI. Previous experimental studies have reported a higher elastic modulus for the outer cortical table than the inner table [13, 54].Third, the assumption of linear, isotropic and homogeneous material properties in the micro-FE model. The accuracy of the model can be further improved by implementing heterogeneous and anisotropic material properties. Nevertheless, the goal of this study was not to optimise the modelling approach but to characterise the mechanical properties of samples using the simplest and most commonly used micro-FE modelling approach. Moreover, a manual segmentation approach was employed for cortical and diploe analysis in this study. Using a fully automatic segmentation technique, problems associated with operator dependencies (precision and bias) are avoided and ensure high consistency between datasets.

5 Conclusion

Using non-destructive approaches, we provided an insight into the mechanical and morphological properties of cranial bone in sagittal CS patients, as well as the relationship between the two. Certain craniofacial procedures, which rely on the malleability of cranial bone are ideally carried out in the first year of patients' life to achieve desired head shape changes. Our results revealed that age was not a determinant of bone microstructure and elastic modulus in sagittal CS patients, which indicates the need for tailoring patient-specific treatments to other parameters. To achieve optimal surgical outcomes, the mechanical and microstructure of the samples should be considered prior to surgery. Since micro-CT cannot be used to assess patients preoperatively, it highlights the need for translatable imaging biomarkers for clinical settings to identify the structural type and determine mechanical properties. This study suggests that morphological parameters such as bone mineral density and cross-sectional thickness [57, 81, 83-86] - which could be measured by routine CT clinical examination - should be further investigated as potential imaging biomarkers.

Acknowledgments

We would like to acknowledge UCL Institute of Orthopaedics and Musculoskeletal Science for mechanical testing instruments and Prof Timothy Arnett for the micro-CT scanner used in this research. This work was supported by the Great Ormond Street Hospital Charity Clinical Research Starter Grant (award number 17DD46) as well as the NIHR GOSH/UCL Biomedical Research Centre Advanced Therapies for Structural Malformations and Tissue Damage pump-prime funding call (grant n. 17DS18), EPSRC grant - the Engineering and Physical Sciences Research Council (EP/N02124X/1), and the European Research Council (ERC-2017-StG-757923). This report incorporates independent research from the National Institute for Health Research Biomedical Research Centre Funding Scheme. The views expressed in this publication are those of the author(s) and not necessarily those of the NHS, the National Institute for Health Research or the Department of Health.

References

1. Governale, L.S., *Craniosynostosis.* Pediatric neurology, 2015. **53**(5): p. 394-401.
2. Ruggiero, F., Wilson, L., James, G., Glass, G., Jeelani, O., Ong, J., Bowman, R., Wyatt, M., Evans, R., Samuels, M. and Hayward, R., *Syndromic craniosynostosis: complexities of clinical care.* Molecular syndromology, 2019. **10**(1-2): p. 83-97.
3. Cohen, S.R., Frank, R.C., Meltzer, H.S. and Levy, M.L., *Craniosynostosis*, in *HANDBOOK OF CRANIOMAXILLOFACIAL SURGERY*. 2014, World Scientific. p. 343-368.
4. Heuzé Y, H.G., Peter I, Richtsmeier JT, Jabs EW., *Closing the gap: genetic and genomic continuum from syndromic to nonsyndromic craniosynostoses.* Current genetic medicine reports, 2014. **2**(3): p. 135-145.
5. RottgeRS, S.A., KiM, P.D., KuMAR, A.R., Cray, J.J., Losee, J.E. and Pollack, I.F., *Cranial vault remodeling for sagittal craniosynostosis in older children.* eurosurgical focus, 2011. **31**(2): p. E3.
6. Rodgers, W., Glass, G., Tahim, A., Ponniah, A., Schievano, S., Borghi, A., James, G., O'Hara, J., Dunaway, D. and Jeelani, O., *Spring assisted cranioplasty for the correction of non-syndromic scaphocephaly: a quantitative analysis of 100 consecutive cases.* British Journal of Oral and Maxillofacial Surgery, 2016. **54**(10): p. e167-e168.
7. David, L.R., Plikaitis, C.M., Couture, D., Glazier, S.S. and Argenta, L.C., *Outcome analysis of our first 75 spring-assisted surgeries for scaphocephaly.* J Journal of Craniofacial Surgery, 2010. **21**(1): p. 3-9.
8. Rodriguez-Florez, N., Bruse, J.L., Borghi, A., Vercruysse, H., Ong, J., James, G., Pennec, X., Dunaway, D.J., Jeelani, N.O. and Schievano, S., *Statistical shape modelling to aid surgical planning: associations between surgical parameters and head shapes following spring-assisted cranioplasty.* International journal of computer assisted radiology surgery, 2017. **12**(10): p. 1739-1749.
9. Borghi, A., Rodriguez-Florez, N., Rodgers, W., James, G., Hayward, R., Dunaway, D., Jeelani, O. and Schievano, S., *Spring assisted cranioplasty: A patient specific computational model.* Medical Engineering & Physics, 2018. **53**: p. 58-65.
10. Zhang, G., Tan, H., Qian, X., Zhang, J., Li, K., David, L.R. and Zhou, X., *A systematic approach to predicting spring force for sagittal craniosynostosis surgery.* Journal of Craniofacial Surgery, 2016. **27**(3): p. 636-643.
11. Rodriguez-Florez N, I.A., Hutchinson JC, Borghi A, James G, Arthurs OJ, Ferretti P, Dunaway D, Schievano S, Jeelani NO, *Cranial bone structure in children with sagittal craniosynostosis: Relationship with surgical outcomes.* Journal of Plastic, Reconstructive & Aesthetic Surgery., 2017. **70**(11): p. 1589-1597.

12. Breisch, E., Haas, E.A., Masoumi, H., Chadwick, A.E. and Krous, H.F., *A morphometric analysis of the infant calvarium and dura.* Forensic science, medicine , and pathology, 2010. **6**(4): p. 249-254.

13. Boruah, S., Paskoff, G.R., Shender, B.S., Subit, D.L., Salzar, R.S. and Crandall, J.R., *Variation of bone layer thicknesses and trabecular volume fraction in the adult male human calvarium.* Bone, 2015. **77**: p. 120-134.

14. Jin, S.W., Sim, K.B. and Kim, S.D., *Development and growth of the normal cranial vault: an embryologic review.* Journal of Korean Neurosurgical Society, 2016. **59**(3): p. 192.

15. Surowiec, R.K., Ram, S., Idiyatullin, D., Goulet, R., Schlecht, S.H., Galban, C.J. and Kozloff, K.M., *In vivo quantitative imaging biomarkers of bone quality and mineral density using multi-band-SWIFT magnetic resonance imaging.* Bone, 2021. **143**: p. 115615.

16. Bianchi, J., Gonçalves, J.R., de Oliveira Ruellas, A.C., Ashman, L.M., Vimort, J.B., Yatabe, M., Paniagua, B., Hernandez, P., Benavides, E., Soki, F.N. and Ioshida, M., *Quantitative bone imaging biomarkers to diagnose temporomandibular joint osteoarthritis.* International Journal of Oral Maxillofacial Surgery, 2021. **50**(2): p. 227-235.

17. Bianchi, J., Gonçalves, J.R., Ruellas, A.C.D.O., Vimort, J.B., Yatabe, M., Paniagua, B., Hernandez, P., Benavides, E., Soki, F.N. and Cevidanes, L.H.S., *Software comparison to analyze bone radiomics from high resolution CBCT scans of mandibular condyles.* Dentomaxillofacial Radiology, 2019. **48**(6): p. 20190049.

18. Rajapakse, C.S., Bashoor-Zadeh, M., Li, C., Sun, W., Wright, A.C. and Wehrli, F.W., *Volumetric cortical bone porosity assessment with MR imaging: validation and clinical feasibility.* Radiology, 2015. **276**(2): p. 526-535.

19. Andrade, A.J., Stock, D., Costi, J.J., Stanley, R., Kelly, N., Hearn, T.C., Oakeshott, R.D. and Spriggins, A.J. *THE IN VIVO INTRAOPERATIVE BIOMECHANICAL PROPERTIES OF ACL GRAFTS*. in *Orthopaedic Proceedings*. 2002. The British Editorial Society of Bone & Joint Surgery.

20. Wang, T., Dionigi, G., Zhao, Y., Zhang, D., Pino, A., Dralle, H., Wu, C.W., Zhou, L. and Sun, H., *Tensile strength analysis of automatic periodic stimulation for continuous intraoperative neural monitoring in a piglet model.* Scientific Reports, 2021. **11**(1): p. 1-6.

21. Chen, Y., Dall, E., Sales, E., Manda, K., Wallace, R., Pankaj, P. and Viceconti, M., *Micro-CT based finite element models of cancellous bone predict accurately displacement once the boundary condition is well replicated: a validation study.* Journal of the mechanical behavior of biomedical materials, 2017. **65**: p. 644-651.

22. Verhulp, E., van Rietbergen, B., Müller, R. and Huiskes, R., *Indirect determination of trabecular bone effective tissue failure properties using micro-finite element simulations.* Journal of biomechanics, 2008. **41**(7): p. 1479-1485.

23. Costa, M.C., Tozzi, G., Cristofolini, L., Danesi, V., Viceconti, M. and Dall'Ara, E., *Micro Finite Element models of the vertebral body: Validation of local displacement predictions.* PloS one, 2017. **12**(7): p. e0180151.

24. He, Z., Chu, L., Liu, X., Han, X., Zhang, K., Yan, M., Li, X. and Yu, Z., *Differences in subchondral trabecular bone microstructure and finite element analysis-based biomechanical properties between osteoporosis and osteoarthritis.* Journal of Orthopaedic Translation, 2020.

25. Wolfram, U., Wilke, H.J. and Zysset, P.K., *Valid μ finite element models of vertebral trabecular bone can be obtained using tissue properties measured with nanoindentation under wet conditions.* Journal of biomechanics, 2010. **43**(9): p. 1731-1737.

26. Granke, M., Coulmier, A., Uppuganti, S., Gaddy, J.A., Does, M.D. and Nyman, J.S., *Insights into reference point indentation involving human cortical bone: sensitivity to tissue anisotropy and mechanical behavior.* Journal of the mechanical behavior of biomedical materials, 2014. **37**: p. 174-185.

27. Bouxsein, M.L., Boyd, S.K., Christiansen, B.A., Guldberg, R.E., Jepsen, K.J. and Müller, R., *Guidelines for assessment of bone microstructure in rodents using micro–computed tomography.* Journal of bone mineral research, 2010. **25**(7): p. 1468-1486.

28. Jenkins, T., Coutts, L.V., Dunlop, D.G., Oreffo, R.O.C., Cooper, C., Harvey, N.C. and Thurner, P.J., *Variability in reference point microindentation and recommendations for testing cortical bone: maximum load, sample orientation, mode of use, sample preparation and measurement spacing.* Journal of the mechanical behavior of biomedical materials, 2015. **42**: p. 311-324.

29. Active Life Scientific, I. *BioDent User Manual*. [cited 2020 02/07]; Available from: http://research.activelifescientific.com/wp-content/uploads/2018/07/BioDent-Hfc-Users-Guide.pdf.

30. Abraham, A.C., Agarwalla, A., Yadavalli, A., Liu, J.Y. and Tang, S.Y., *Microstructural and compositional contributions towards the mechanical behavior of aging human bone measured by cyclic and impact reference point indentation.* Bone, 2016. **87**: p. 37-43.

31. Oliver, W.C.a.P., G.M., *An improved technique for determining hardness and elastic modulus using load and displacement sensing indentation experiments.* Journal of materials research, 1992. **7**(6): p. 1564-1583.

32. Persing, J.A., *MOC-PS (SM) CME article: management considerations in the treatment of craniosynostosis.* Plastic

reconstructive surgery, 2008. **121**(4): p. 1-11.

33. Windh, P., Davis, C., Sanger, C., Sahlin, P. and Lauritzen, C., *Spring-assisted cranioplasty vs pi-plasty for sagittal synostosis-a long term follow-up study.* Journal of Craniofacial Surgery, 2008. **19**(1): p. 59-64.

34. Leppänen, O.V., Sievänen, H. and Järvinen, T.L., *Biomechanical testing in experimental bone interventions—May the power be with you.* Journal of biomechanics, 2008. **41**(8): p. 1623-1631.

35. Prodinger, P.M., Foehr, P., Bürklein, D., Bissinger, O., Pilge, H., Kreutzer, K., von Eisenhart-Rothe, R. and Tischer, T., *Whole bone testing in small animals: systematic characterization of the mechanical properties of different rodent bones available for rat fracture models.* 2018. **23**(1): p. 1-11.

36. Schriefer, J.L., Robling, A.G., Warden, S.J., Fournier, A.J., Mason, J.J. and Turner, C.H., *A comparison of mechanical properties derived from multiple skeletal sites in mice.* Journal of biomechanics, 2005. **38**(3): p. 467-475.

37. Spatz, H.C.a.V., J.F.V., *Young's moduli and shear moduli in cortical bone.* Proceedings of the Royal Society of London. Series B: Biological Sciences, 1996. **263**(1368): p. 287-294.

38. Young, W.C., Budynas, R.G. and Sadegh, A.M., *Roark's formulas for stress and strain*. Vol. 7. 2002: McGraw-hill New York.

39. Wallace, R.J., Pankaj, P. and Simpson, A.H.R.W., *Major source of error when calculating bone mechanical properties.* Journal of Bone Mineral Research, 2014. **29**(12): p. 2697-2697.

40. Kourtis, L.C., Carter, D.R. and Beaupre, G.S., *Improving the estimate of the effective elastic modulus derived from three-point bending tests of long bones.* Annals of biomedical engineering, 2014. **42**(8): p. 1773-1780.

41. Osuna, L.G.G., Soares, C.J., Vilela, A.B.F., Irie, M.S., Versluis, A. and Soares, P.B.F., *Influence of bone defect position and span in 3-point bending tests: experimental and finite element analysis.* Brazilian Oral Research, 2020. **35**.

42. Hubbard, R.P., *Flexure of layered cranial bone.* Journal of Biomechanics, 1971. **4**(4): p. 251-263.

43. Delille, R., Lesueur, D., Potier, P., Drazetic, P. and Markiewicz, E. , *Experimental study of the bone behaviour of the human skull bone for the development of a physical head model.* International Journal of Crashworthiness, 2007. **12**(2): p. 101-108.

44. McPherson, G.K.a.K., T.J., *The elastic modulus of fetal cranial bone: a first step towards an understanding of the biomechanics of fetal head molding.* Journal of Biomechanics, 1980. **13**(1): p. 9-16.

45. Coats, B.a.M., S.S., *Material properties of human infant skull and suture at high rates.* Journal of neurotrauma, 2006. **23**(8): p. 1222-1232.

46. Rahmoun, J., Auperrin, A., Delille, R., Naceur, H. and Drazetic, P., *Characterization and micromechanical modeling of the human cranial bone elastic properties.* Mechanics Research Communications, 2014. **60**: p. 7-14.

47. Lee, J.H.C., Ondruschka, B., Falland-Cheung, L., Scholze, M., Hammer, N., Tong, D.C. and Waddell, J.N., *An Investigation on the Correlation between the Mechanical Properties of Human Skull Bone, Its Geometry, Microarchitectural Properties, and Water Content.* Journal of healthcare engineering, 2019. **2019**.

48. Wang, J., Zou, D., Li, Z., Huang, P., Li, D., Shao, Y., Wang, H. and Chen, Y., *Mechanical properties of cranial bones and sutures in 1–2-year-old infants.* Medical science monitor: international medical journal of experimental clinical research, 2014. **20**: p. 1808.

49. Margulies, S.S.a.T., K.L., *Infant skull and suture properties: measurements and implications for mechanisms of pediatric brain injury.* J. Biomech. Eng., 2000. **122**(4): p. 364-371.

50. Idkaidek, A., Agarwal, V. and Jasiuk, I., *Finite element simulation of Reference Point Indentation on bone.* Journal of the mechanical behavior of biomedical materials, 2017. **65**: p. 574-583.

51. Hoffseth, K., Randall, C., Hansma, P. and Yang, H.T, *Study of indentation of a sample equine bone using finite element simulation and single cycle reference point indentation.* Journal of the mechanical behavior of biomedical materials, 2015. **42**: p. 282-291.

52. Melvin, J.W., Robbins, D.H. and Roberts, V.L., *The mechanical behavior of the diploë layer of the human skull in compression.* Dev. Mech, 1969. **5**: p. 811-818.

53. Kleiven, S.a.v.H., H., *Consequences of head size following trauma to the human head.* Journal of biomechanics, 2002. **35**(2): p. 153-160.

54. Peterson, J.a.D., P.C., *Material properties of the human cranial vault and zygoma.* The Anatomical Record Part A: Discoveries in Molecular, Cellular,Evolutionary Biology: An Official Publication of the American Association of Anatomists, 2003. **274**(1): p. 785-797.

55. Davis, M.T., Loyd, A.M., Shen, H.Y.H., Mulroy, M.H., Nightingale, R.W., Myers, B.S. and Bass, C.D., *The mechanical and morphological properties of 6 year-old cranial bone.* Journal of biomechanics, 2012. **45**(15): p. 2493-2498.

56. Williams, P., *Warwick R. Gray's anatomy. 36th British Edition*. 1980, Philadelphia: WB Saunders Co/Churchill Livingstone.

57. Delye, H., Clijmans, T., Mommaerts, M.Y., Sloten, J.V. and Goffin, J., *Creating a normative database of age-specific 3D geometrical data, bone density, and bone thickness of the developing skull: a pilot study.* Journal of Neurosurgery: Pediatrics, 2015. **16**(6): p. 687-702.

58. de Souza Fernandes, A.C., Neto, A.I.T., de Freitas, A.C. and de Moraes, M., *Dimensional analysis of the parietal bone in areas of surgical interest and relationship between parietal thickness and cephalic index.* Journal of oral maxillofacial surgery, 2011. **69**(11): p. 2930-2935.

59. Moreira-Gonzalez, A., Papay, F.E. and Zins, J.E., *Calvarial thickness and its relation to cranial bone harvest.* Plastic reconstructive surgery, 2006. **117**(6): p. 1964-1971.

60. Pensler, J.a.M., J.G. , *The calvarial donor site: an anatomic study in cadavers.* Plastic and reconstructive surgery, 1985. **75**(5): p. 648-651.

61. Hwang, K., Kim, J.H. and Baik, S.H., *Thickness map of parietal bone in Korean adults.* The Journal of craniofacial surgery, 1997. **8**(3): p. 208-212.

62. Boulet, S.L., Rasmussen, S.A. and Honein, M.A., *A population-based study of craniosynostosis in metropolitan Atlanta, 1989–2003.* American Journal of Medical Genetics Part A, 2008. **146**(8): p. 984-991.

63. Lee, H.Q., Hutson, J.M., Wray, A.C., Lo, P.A., Chong, D.K., Holmes, A.D. and Greensmith, A.L., *Changing epidemiology of nonsyndromic craniosynostosis and revisiting the risk factors.* Journal of Craniofacial Surgery, 2012. **23**(5): p. 1245-1251.

64. Kimonis, V., Gold, J.A., Hoffman, T.L., Panchal, J. and Boyadjiev, S.A., *Genetics of Craniosynostosis.* Seminars in Pediatric Neurology, 2007. **14**(3): p. 150-161.

65. French, L.R., Jackson, I.T. and Melton III, L.J., *A population-based study of craniosynostosis.* Journal of clinical epidemiology, 1990. **43**(1): p. 69-73.

66. Graham Jr, J.M., deSaxe, M. and Smith, D.W., *Sagittal craniostenosis: fetal head constraint as one possible cause.* The Journal of pediatrics, 1979. **95**(5): p. 747-750.

67. Sloan, G.M., Wells, K.C., Raffel, C. and McComb, J.G., *Surgical treatment of craniosynostosis: outcome analysis of 250 consecutive patients.* Pediatrics, 1997. **100**(1): p. e2-e2.

68. Lin, I.C., Slemp, A.E., Hwang, C., Sena-Esteves, M., Nah, H.D. and Kirschner, R.E., *Dihydrotestosterone stimulates proliferation and differentiation of fetal calvarial osteoblasts and dural cells and induces cranial suture fusion.* Plastic reconstructive surgery, 2007. **120**(5): p. 1137-1147.

69. Park, S.S., Beyer, R.P., Smyth, M.D., Clarke, C.M., Timms, A.E., Bammler, T.K., Stamper, B.D., Mecham, B.H., Gustafson, J.A. and Cunningham, M.L., *Osteoblast differentiation profiles define sex specific gene expression patterns in craniosynostosis.* Bone, 2015. **76**: p. 169-176.

70. Kim, D.G., Christopherson, G.T., Dong, X.N., Fyhrie, D.P. and Yeni, Y.N., *The effect of microcomputed tomography scanning and reconstruction voxel size on the accuracy of stereological measurements in human cancellous bone.* Bone, 2004. **35**(6): p. 1375-1382.

71. Palacio-Mancheno, P.E., Larriera, A.I., Doty, S.B., Cardoso, L. and Fritton, S.P., *3D assessment of cortical bone porosity and tissue mineral density using high-resolution µCT: effects of resolution and threshold method.* Journal of Bone Mineral Research, 2014. **29**(1): p. 142-150.

72. Zhai, X., Nauman, E.A., Moryl, D., Lycke, R. and Chen, W.W., *The effects of loading-direction and strain-rate on the mechanical behaviors of human frontal skull bone.* Journal of the Mechanical Behavior of Biomedical Materials, 2020. **103**: p. 103597.

73. Morgan, E.F., Unnikrisnan, G.U. and Hussein, A.I., *Bone mechanical properties in healthy and diseased states.* Annual review of biomedical engineering, 2018. **20**: p. 119-143.

74. Schaffler, M.B.a.B., D.B., *Stiffness of compact bone: effects of porosity and density.* Journal of biomechanics, 1988. **21**(1): p. 13-16.

75. Boughton, O.R., Ma, S., Cai, X., Yan, L., Peralta, L., Laugier, P., Marrow, J., Giuliani, F., Hansen, U., Abel, R.L. and Grimal, Q., *Computed tomography porosity and spherical indentation for determining cortical bone millimetre-scale mechanical properties.* Scientific reports, 2019. **9**(1): p. 1-15.

76. Jorgenson, B.L., Buie, H.R., McErlain, D.D., Sandino, C. and Boyd, S.K., *A comparison of methods for in vivo assessment of cortical porosity in the human appendicular skeleton.* Bone, 2015. **73**: p. 167-175.

77. Tjong, W., Nirody, J., Burghardt, A.J., Carballido-Gamio, J. and Kazakia, G.J., *Structural analysis of cortical porosity applied to HR-pQCT data.* Medical physics, 2014. **41**(1): p. 013701.

78. Lee, S., Chung, C.K., Oh, S.H. and Park, S.B., *Correlation between bone mineral density measured by dual-energy X-ray absorptiometry and Hounsfield units measured by diagnostic CT in lumbar spine.* Journal of Korean Neurosurgical Society, 2013. **54**(5): p. 384.

79. Schreiber, J.J., Anderson, P.A., Rosas, H.G., Buchholz, A.L. and Au, A.G., *Hounsfield units for assessing bone mineral density and strength: a tool for osteoporosis management.* JBJS, 2011. **93**(11): p. 1057-1063.

80. Choi, M.K., Kim, S.M. and Lim, J.K., *Diagnostic efficacy of Hounsfield units in spine CT for the assessment of real bone mineral density of degenerative spine: correlation study between T-scores determined by DEXA scan and Hounsfield units from CT.* Acta Neurochirurgica, 2016. **158**(7): p. 1421-1427.

81. Schreiber, J.J., Anderson, P.A. and Hsu, W.K., *Use of computed tomography for assessing bone mineral density.* Neurosurgical focus, 2014. **37**(1): p. E4.

82. Öhman, C., Dall'Ara, E., Baleani, M., Jan, S.V.S. and Viceconti, M., *The effects of embalming using a 4% formalin solution on the compressive mechanical properties of human cortical bone.* Clinical biomechanics, 2008. **23**(10): p. 1294-1298.

83. Mazonakis, M.a.D., J., *Computed tomography: What and how does it measure?* European journal of radiology, 2016. **85**(8): p. 1499-1504.

84. Lillie, E.M., Urban, J.E., Weaver, A.A., Powers, A.K. and Stitzel, J.D., *Estimation of skull table thickness with clinical CT and validation with microCT.* Journal of Anatomy, 2015. **226**(1): p. 73-80.

85. Stone, J.L., Gulabani, A., Gorelick, G., Vannemreddy, S.N. and Vannemreddy, P.S., *Frontolateral pins for halo ring placement: reassessment of a common neurosurgical procedure with CT measurements of skull thickness.* Journal of Neurosurgery: Spine, 2013. **19**(6): p. 744-749.

86. Pedro, D.F., Junichi, Y., Julio, D., Carlos, B., Francisco, S.C., Jorge, K. and Federico, C., *Analysis of skull bone thickness during growth: an anatomical guide for safe pin placement in halo fixation.* J European Spine Journal, 2020: p. 1-6.

Author statement

Sara Ajami: Conceptualization, Methodology, Validation, Investigation, Resources, Writing - Original Draft, Writing - Review & Editing

Naiara Rodriguez-Florez: Conceptualization**,** Methodology, Writing - Review & Editing

Juling Ong: Supervision, Resources, Writing – review & editing, Funding acquisition

Noor ul Owase Jeelani: Supervision, Resources, Writing – review & editing, Funding acquisition

David Dunaway: Supervision, Resources, Writing – review & editing, Funding acquisition

Greg James: Supervision, Resources, Writing – review & editing

Freida Angullia: Resources, Writing – review & editing

Curtis Burden: Resources, Writing – review & editing

Selim Bozkurt: Writing – review & editing

Amel Ibrahim: Investigation

Patrizia Ferretti: Supervision, Writing – review & editing

Silvia Schievano: Supervision, Writing – review & editing, Funding acquisition

Alessandro Borghi: Conceptualization, Methodology, Validation, Writing - Review & Editing, Project administration, Funding acquisition

Declaration of interests

☒ The authors declare that they have no known competing financial interests or personal relationships that could have appeared to influence the work reported in this paper.

☐The authors declare the following financial interests/personal relationships which may be considered as potential competing interests: